Supplemental Material Information

Authors: Shaomin Yang[1†], Xiaolian Liu[1†], Mei Wang[1†], Di Cao[1†], Dabbu Kumar Jaijyan[2], Nicole Enescu[2], Jian Liu[3], Songbin Wu[4], Sashuang Wang[4], Wuping Sun[4], Lizu Xiao[4], Yaolan Li[1], Hong Zhou[5], Sanjay Tyagi[6,7], Jianguo Wu[1], Qiyi Tang[5], Hua Zhu[2*]

Affiliations:

[1] Jinan University, Guangzhou, Guangdong, 510632, China.

[2] Department of Microbiology and Molecular Genetics, New Jersey Medical School, Rutgers University, 225 Warren Street, Newark, NJ 070101, USA.

[3] School of Biological Sciences and Biotechnology, Minnan Normal University, Zhangzhou 363000, China.

[4] Department of Pain Medicine and Shenzhen Municipal Key Laboratory for Pain Medicine, Shenzhen Nanshan People's Hospital, The 6th Affiliated Hospital of Shenzhen University Health Science Center, Shenzhen, China.

[5] Department of Microbiology, Howard University College of Medicine, 520 W Street NW Washington, DC 20059, USA.

[6]Public Health Research Institute, New Jersey Medical School, Newark NJ07103

[7]Department of Medicine, New Jersey Medical School, Rutgers University.

†Co-first authors, these authors contributed equally to this work.

*Correspondence to: hua.zhu@rutgers.edu

Figure S1. Mapping statistics.

(A-F) Read counts from HCMV TB40/E strain-infected EC **(A)**, NPCs **(B)**, HFF **(C)**, HAN strain infected-HELF **(D)**, KSHV BCBL1 strain-infected-B cell lymphoma **(E),** and EBV Akata strain-infected B cell lymphoma **(F)** related RNA-Seq. **(G-I)** Genome coverage of HCMV HAN strain-infected HELF **(G)**, KSHV BCBL1 strain-infected B cell lymphoma **(H),** and EBV Akata strain-infected B cell lymphoma **(I)**. **(J-K)** Frequency of circularization events in KSHV **(J)** and EBV **(K)**. Counts of BSJ-spanning reads of circRNAs (starting from a coordinate in the x-axis and ending at a coordinate in the y-axis) indicated by color. The circRNA start/stop positions are shown as histograms on the x- and y-axes. Ranked expression levels of *de novo* identified circRNAs from HCMV and human genomes. The labels of the top 10 circRNAs are shown according to their genome positions. The complete list of splice sites is provided in Data S1.

Figure S2. Genome organization and Reconstructed circRNAs from the HCMV HAN strain.

The ORFs are color-coded according to the growth properties of their corresponding virus gene-deletion mutants. Variation multigene segment of the HAN strain: ~15 kb (176,729 to 191,263 bp). The relative expression levels of circRNAs are indicated by the colors at the bottom. Reconstruction of full-length circRNAs and partially assembled circRNAs indicated by “Full” and “Break”, respectively. The complete list of splice sites is provided in Data S1.

Figure S3. Inverse RT-PCR used for subcloning and sequencing.

(A) Inverse RT-PCR result of the HCMV clinical strains TB40/E and Toledo and a laboratory strain with selected primer sets**. (B-C)** The expression of HCMV circRNAs in HFF, HELF**,** and U373 cells at different infection time points. **(D)** Inverse RT-PCR on RNA treated with or without RNase R. GAPDH and HCMV linear RNA, IE1/2, early gene (UL105), and late (UL111A) gene**. (E)** Relative resistance ability to RNase R of linear RNA and circRNAs. The value was normalized to the corresponding sample without RNase R treatment. **(F-I)** BSJ breakpoints are indicated by dashed lines. Donor (green), acceptor (blue) sequences, and

downstream/upstream sequences (grey) flanking the junction were aligned with the BSJ sequence. **(J)** Sanger sequencing result of three different divergent primers amplified BSJ#5 for constructing full-length of circRNA#5.

Figure S4. Demonstration of the high level of specificity of the spot counting algorithm and the detection of human circHIPK3 using smFISH/ampFISH.

(A) Demonstration of high specificity of spot counting algorithm. Analysis of same field of cells as in Figure 5 is presented. A yellow circle is placed over each detected spot. The circles and cell boundaries are placed over a compressed z-stacks of Cy5 images filtered by a Laplacian filter. The right panels represent enlargements of indicated regions from the middle panels that were designed to show the detected spots within each yellow circle. The contrast levels of the underlaying images may appear different from the raw images in Figure 5 because of processing by the Laplacian filter. **(B)** The detection of human circHIPK3 using ampFISH. Linear HIPK3 transcript was detected using a smFISH probe set comprising of 48 probes and circHIPK3 was detected using a ampFISH probe pair against the sequences on either side of BSJ. Images on the left are for the GFP (depicting HCMV) and DAPI channels and ones on the right are merged z-stacks for Cy5 channels for the same fields. The bottom panel shows a pair of cells in which smFISH signal from linear HIPK3 mRNA is shown in green, ampFISH signal from circHIPK3 RNA is shown in red and the nuclei in blue. smFISH probes were designed so that they would not bind in the region of linear HIPK3 RNA that is common between the linear and circular RNA species. In general, no colocalization between the spots of two colors was observed. **(C-D)** Number of mRNA spots corresponding to single mRNA molecules are shown for indicated categories of cells. Two-tailed unpaired t test. *$p < 0.05$, **$p < 0.01$, ***$p < 0.001$ mock vs. infected group; ### $p < 0.001$ without RNase R treatment vs. with RNase R treatment group. Data presented as mean ± S.E.M. The number of cells analyzed (n) are indicated in labels of the bars.

Figure S5. The circRNA-miRNA-mRNA network of HCMV circRNA is involved in the competitive endogenous RNA coregulatory network.

(A) “DNA replication” GO Biological Process term, **(B)** “ATPase activity” GO Cellular Component term, **(C)** “Replication fork” GO Molecular Function term, **(D)** “Cell cycle” KEGG pathway term.

Data S1. BSJs called by CIRI2 and reconstructed circRNAs predicted by CIRI-full

Data S2. Experimentally confirmed HCMV circRNAs, Homology and complementarity analysis of simulated circRNAs and experimentally confirmed HCMV circRNAs

Data S3. Functional annotation of HCMV circRNAs in regulating parental gene

Data S4. Human miRNAs interacting with full-length HCMV circRNAs predicted by miRanda

Figure S1

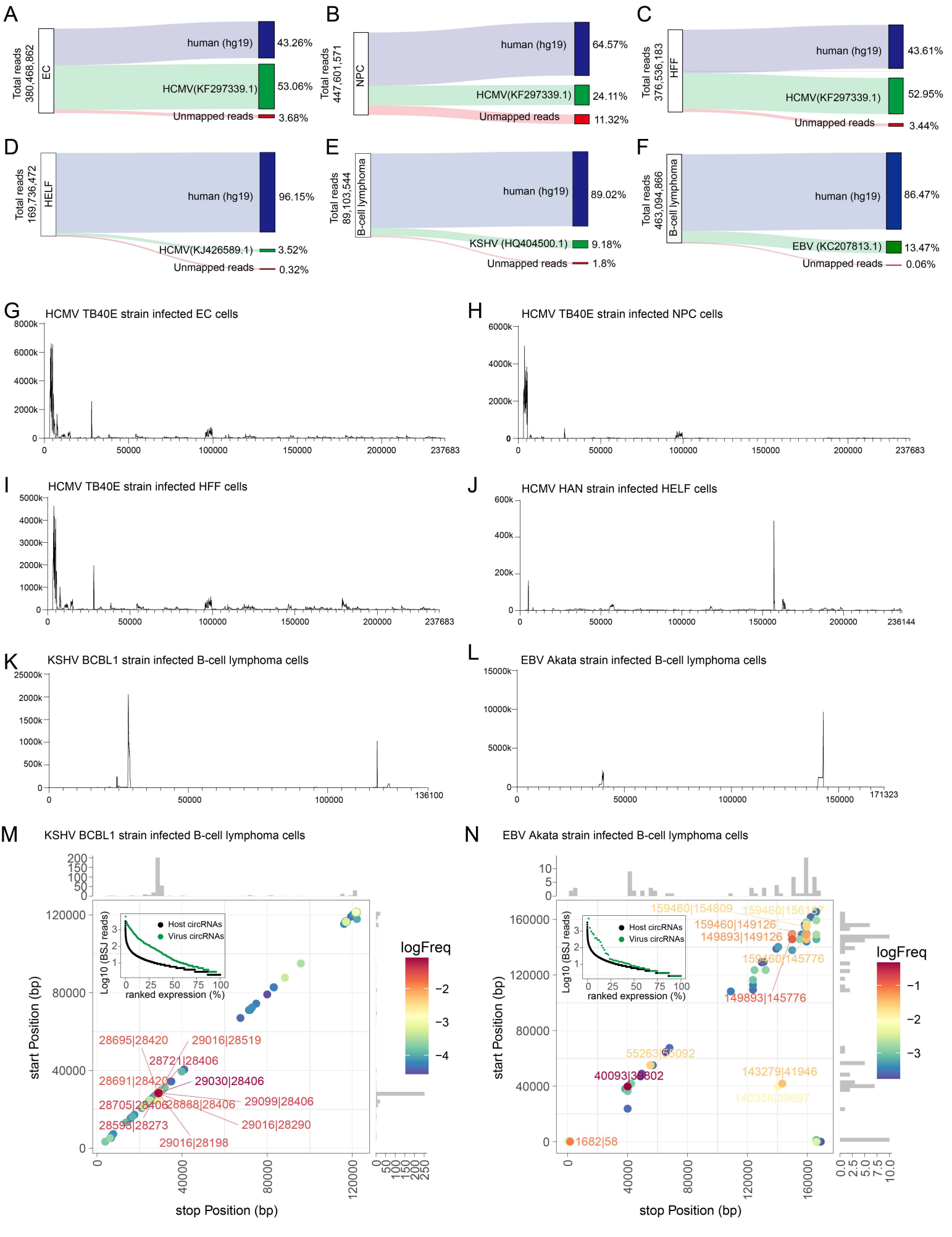
A
Total reads 380,468,862
EC
human (hg19) 43.26%
HCMV(KF297339.1) 53.06%
Unmapped reads 3.68%
B
Total reads 447,601,571
NPC
human (hg19) 64.57%
HCMV(KF297339.1) 24.11%
Unmapped reads 11.32%
C
Total reads 376,536,183
HFF
human (hg19) 43.61%
HCMV(KF297339.1) 52.95%
Unmapped reads 3.44%
D
Total reads 169,736,472
HELF
human (hg19) 96.15%
HCMV(KJ426589.1) 3.52%
Unmapped reads 0.32%
E
Total reads 89,103,544
B-cell lymphoma
human (hg19) 89.02%
KSHV (HQ404500.1) 9.18%
Unmapped reads 1.8%
F
Total reads 463,094,866
B-cell lymphoma
human (hg19) 86.47%
EBV (KC207813.1) 13.47%
Unmapped reads 0.06%
G
HCMV TB40E strain infected EC cells
H
HCMV TB40E strain infected NPC cells
I
HCMV TB40E strain infected HFF cells
J
HCMV HAN strain infected HELF cells
K
KSHV BCBL1 strain infected B-cell lymphoma cells
L
EBV Akata strain infected B-cell lymphoma cells
M
KSHV BCBL1 strain infected B-cell lymphoma cells
Host circRNAs
Virus circRNAs
Log10 (BSJ reads)
ranked expression (%)
logFreq
28695|28420
29016|28519
28721|28406
28691|28420
29030|28406
28705|28406
28888|28406
29099|28406
28595|28273
29016|28290
29016|28198
start Position (bp)
stop Position (bp)
N
EBV Akata strain infected B-cell lymphoma cells
159460|154809
159460|156187
159460|149126
149893|149126
159460|145776
149893|145776
55263|55092
40093|39802
143279|41946
140356|39697
1682|58

Figure S2

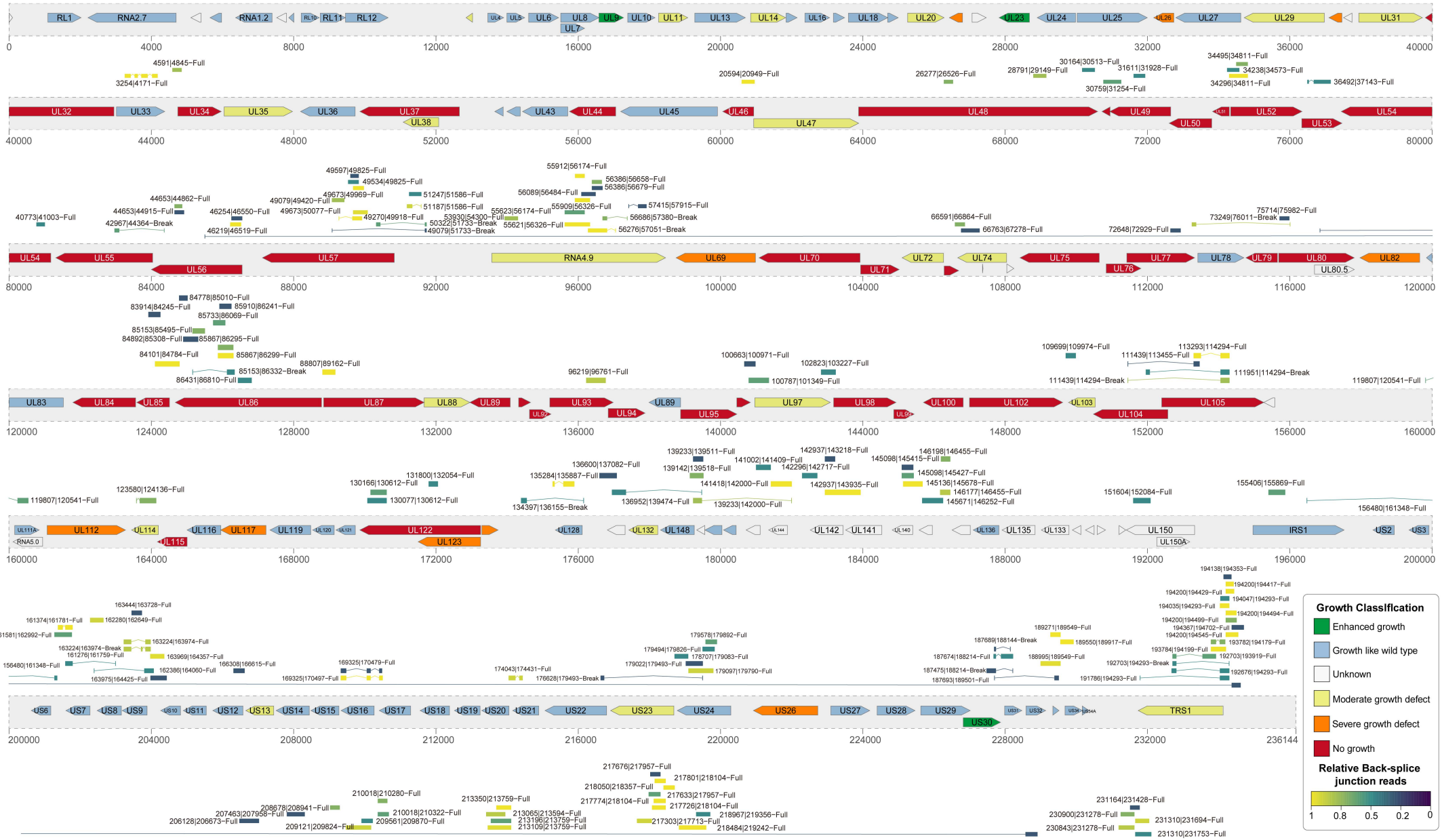
RL1
RNA2.7
RNA1.2
RL1b
RL11
RL12
UL4
UL5
UL6
UL8
UL7
UL9
UL10
UL11
UL13
UL14
UL16
UL18
UL20
UL23
UL24
UL25
UL26
UL27
UL29
UL31
UL32
UL33
UL34
UL35
UL36
UL37
UL38
UL43
UL44
UL45
UL46
UL47
UL48
UL49
UL50
UL51
UL52
UL53
UL54
UL55
UL56
UL57
RNA4.9
UL69
UL70
UL71
UL72
UL74
UL75
UL76
UL77
UL78
UL79
UL80
UL80.5
UL82
UL83
UL84
UL85
UL86
UL87
UL88
UL89
UL92
UL93
UL94
UL89
UL95
UL97
UL98
UL99
UL100
UL102
UL103
UL104
UL105
UL111A
RNA5.0
UL112
UL114
UL115
UL116
UL117
UL119
UL120
UL121
UL122
UL123
UL128
UL132
UL148
UL144
UL142
UL141
UL140
UL136
UL135
UL133
UL150
UL150A
IRS1
US2
US3
US6
US7
US8
US9
US10
US11
US12
US13
US14
US15
US16
US17
US18
US19
US20
US21
US22
US23
US24
US26
US27
US28
US29
US30
US31
US32
US34
US34A
TRS1
Growth Classification
Enhanced growth
Growth like wild type
Unknown
Moderate growth defect
Severe growth defect
No growth
Relative Back-splice junction reads
1
0.8
0.5
0.2
0

Figure S3

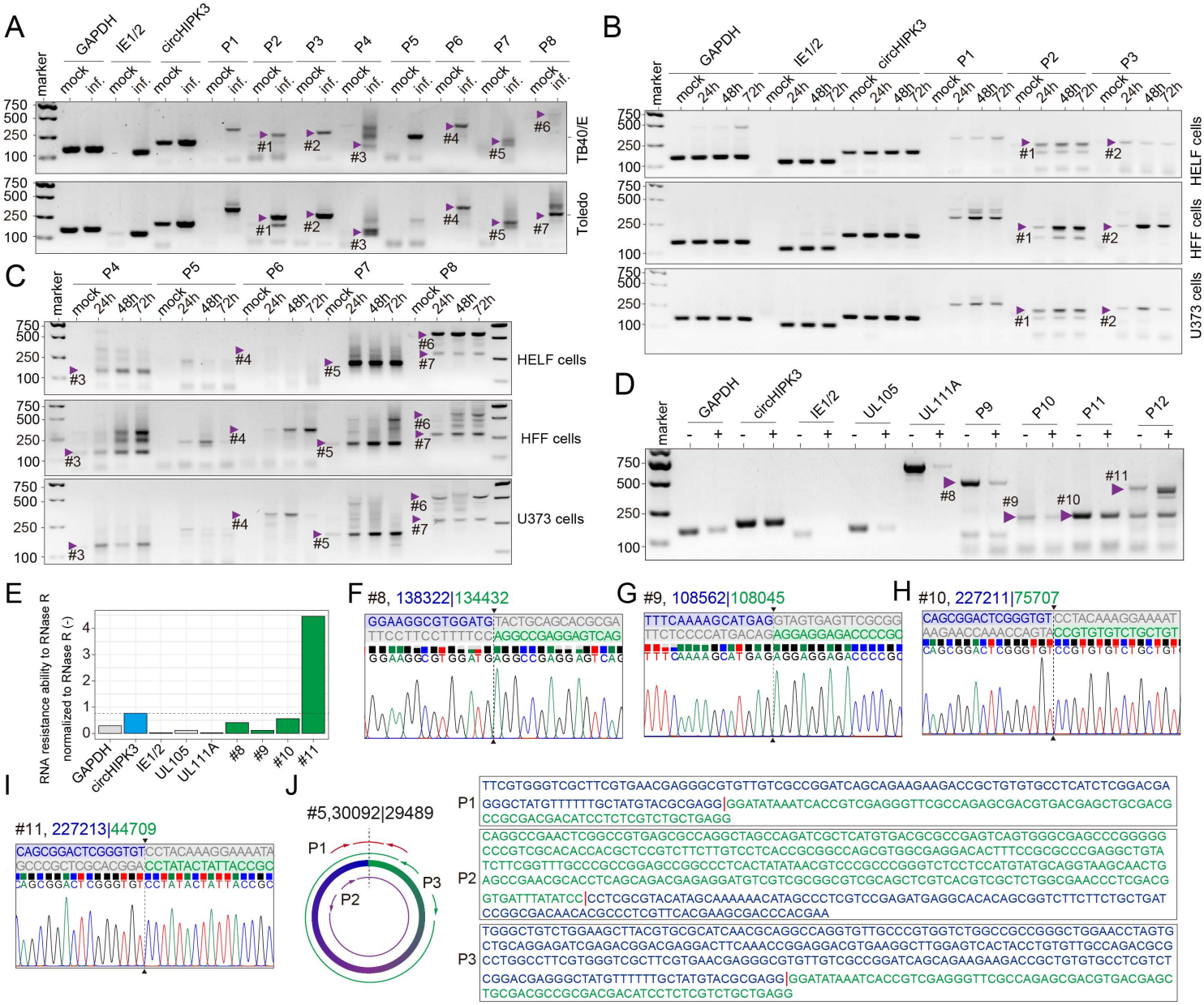
A
B
C
D
E
F
G
H
I
J
GAPDH
IE1/2
circHIPK3
P1
P2
P3
P4
P5
P6
P7
P8
marker
mock
inf.
TB40/E
Toledo
HELF cells
HFF cells
U373 cells
P9
P10
P11
P12
UL105
UL111A
RNA resistance ability to RNase R normalized to RNase R (-)
#8, 138322|134432
#9, 108562|108045
#10, 227211|75707
#11, 227213|44709
#5,30092|29489
P1
P2
P3

Figure S4

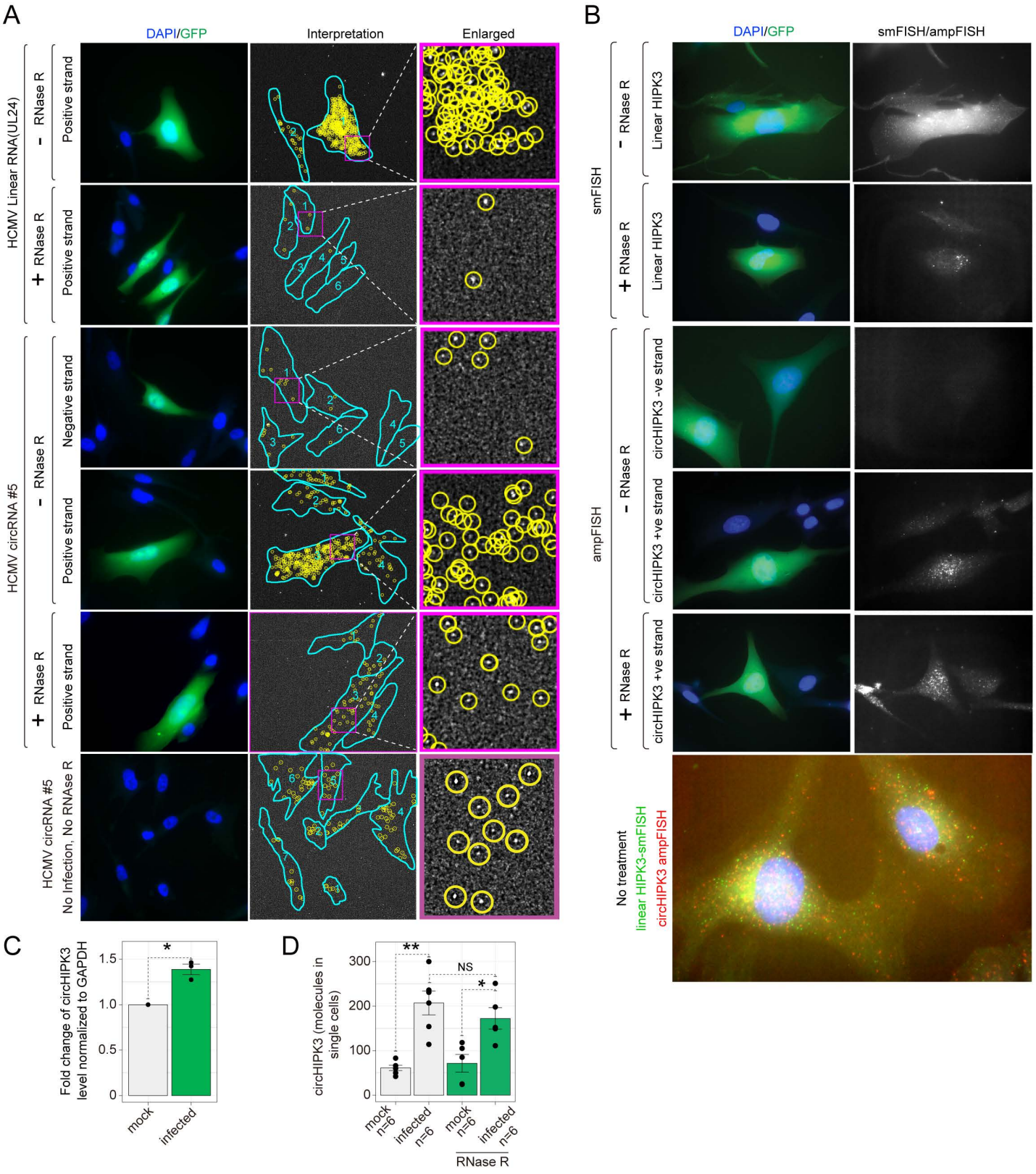
A
DAPI/GFP
Interpretation
Enlarged
HCMV Linear RNA(UL24)
- RNase R
Positive strand
+ RNase R
Positive strand
HCMV circRNA #5
- RNase R
Negative strand
Positive strand
+ RNase R
Positive strand
HCMV circRNA #5
No Infection, No RNAse R
B
DAPI/GFP
smFISH/ampFISH
smFISH
- RNase R
Linear HIPK3
+ RNase R
Linear HIPK3
ampFISH
- RNase R
circHIPK3 -ve strand
circHIPK3 +ve strand
+ RNase R
circHIPK3 +ve strand
No treatment
linear HIPK3-smFISH
circHIPK3 ampFISH
C
Fold change of circHIPK3 level normalized to GAPDH
1.5
1.0
0.5
0
*
mock
infected
D
circHIPK3 (molecules in single cells)
300
200
100
0
**
NS
*
mock n=6
infected n=6
mock n=6
infected n=6
RNase R

Figure S5

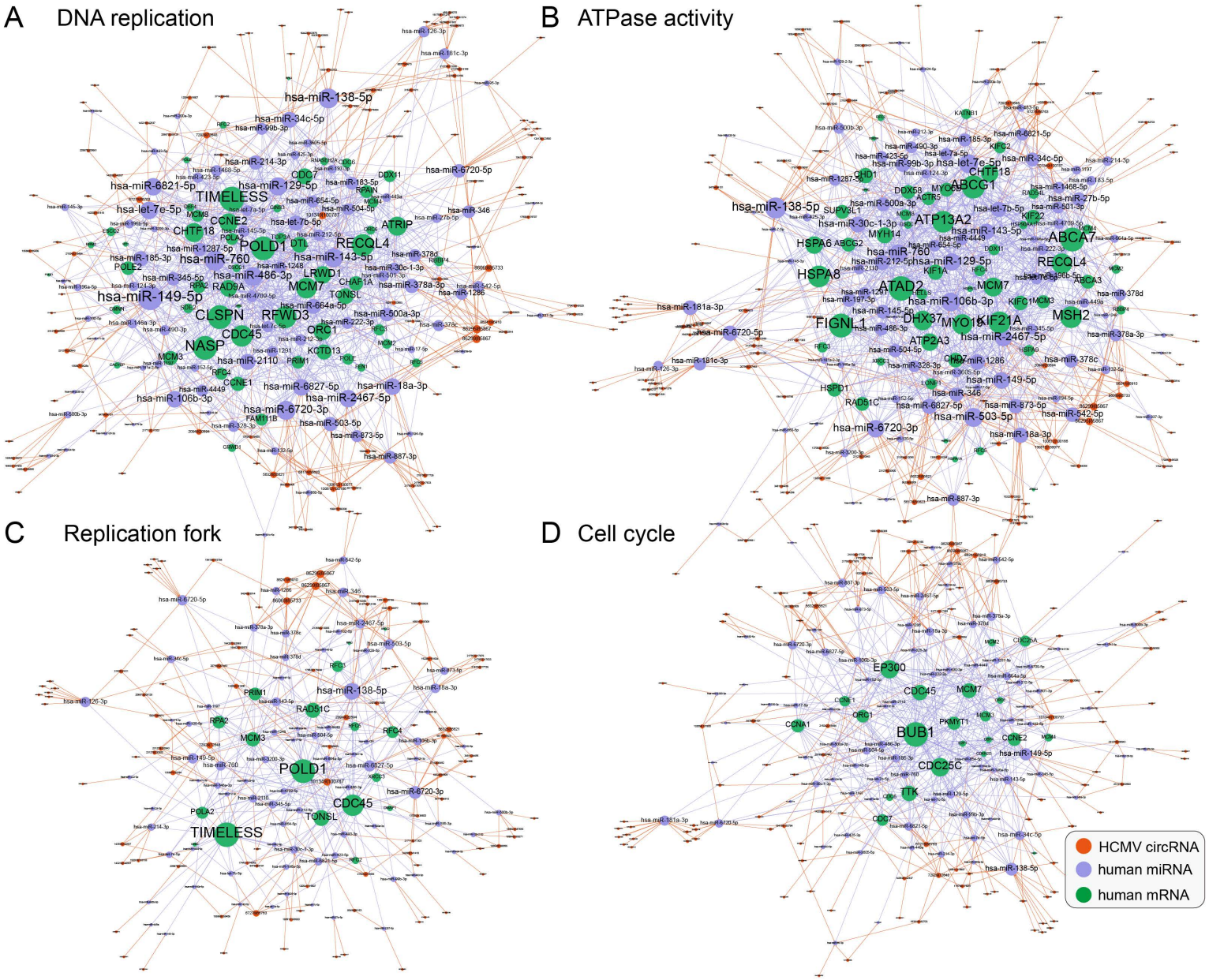
A DNA replication
B ATPase activity
C Replication fork
D Cell cycle
HCMV circRNA
human miRNA
human mRNA